Journal of Earth Science, *Vol. 30*, *No. 2*, *p. 335–347*, *April 2019* *ISSN 1674-487X*
Printed in China
https://doi.org/10.1007/s12583-018-1203-8

Geochronology, Geochemistry, and Hf Isotopic Compositions of Monzogranites and Mafic-Ultramafic Complexes in the Maxingdawannan Area, Eastern Kunlun Orogen, Western China: Implications for Magma Sources, Geodynamic Setting, and Petrogenesis

Jiaming Yan[1], **Guosheng Sun**[*1], **Fengyue Sun**[1], **Liang Li**[1], **Haoran Li**[1], **Zhenhua Gao**[2], **Lei Hua**[2], **Zhengping Yan**[1, 3]

1. *College of Earth Sciences*, *Jilin University*, *Changchun* 130061, *China*
2. *The Eighth Institute of Shandong Geological Exploration*, *Rizhao* 276000, *China*
3. *Qinghai Provincial Bureau of Ferrous Metal and Geological Exploration*, *Xining* 810007, *China*

Jiaming Yan: https://orcid.org/0000-0002-4065-9091; Guosheng Sun: https://orcid.org/0000-0001-7682-4995

ABSTRACT: This paper presents zircon U-Pb-Hf isotopic compositions and whole-rock geochemical data for monzogranites and mafic-ultramafic complexes of the Maxingdawannan area in the western end of the east Kunlun orogenic belt, western China. The data are used to determine the ages, petrogenesis, magma sources, and geodynamic setting of the studied rocks. U-Pb zircon dating indicates that monzogranites and gabbros of the complexes were emplaced at 399 and 397 Ma, respectively. The monzogranites are shoshonitic, with high SiO_2, Al_2O_3 and total-alkali contents, and low TFeO, MgO, TiO_2 and P_2O_5 contents. The mafic-ultramafic complexes are characterized by low SiO_2 contents. The monzogranites display enrichment in light rare-earth elements (LREE) and large-ion lithophile elements (LILE), depletion in heavy REEs (HREE) and high-field-strength elements (HFSE), and negative Eu anomalies (Eu/Eu*=0.36–0.48). The mafic-ultramafic complexes are also enriched in LREEs and LILEs, and depleted in HREEs and HFSEs, with weak Eu anomalies (Eu/Eu*=0.84–1.16). Zircon $\varepsilon_{Hf}(t)$ values for the monzogranites and mafic-ultramafic complexes range from -6.68 to 1.11 and -1.81 to 6.29, with zircon model ages of 1 812–1 319 Ma (T_{DM2}) and 1 087–769 Ma (T_{DM1}), respectively. Hf isotopic data indicate that primary magmas of the monzogranites are originated from partial melting of ancient lower crust during the Paleo-Mesoproterozoic, with a juvenile-crust component. Primitive magmas of the mafic-ultramafic complexes are likely originated from a depleted-mantle source modified by slab-derived fluids and contaminated by crustal components. Geochemical data and the geological setting indicate that Devonian intrusions in the Maxingdawannan area are related to northward subduction of the Proto-Tethys oceanic lithosphere.

KEY WORDS: geochronology, geochemistry, Hf isotopes, Maxingdawannan, Proto-Tethys Ocean.

0 INTRODUCTION

The east Kunlun orogenic belt (EKOB) is a part of the western segment of the central orogenic belt, China, and is one of the primary tectono-magmatic belts of the northern Tibetan Plateau. Multistage tectono-magmatic events have affected the region, including the closure of ancient oceans, continental convergence, accretionary, collisional and superimposed orogenies, and changes in tectonic regime (Chen et al., 2018; Zhao et al., 2018; Deng et al., 2015, 2014a, b, 2012; Dai et al., 2013). The EKOB is situated in a pivotal location at the junction between the Tethyan and Pan-Asian tectonic domains (Jiang et al., 2013). From the Early Paleozoic to Late Triassic, it was affected by the Proto- and Paleo-Tethys orogenies (Chen et al., 2015; Yang et al., 1996). Multistage tectono-magmatic events occurred during subduction of the Proto-Tethys oceanic lithosphere. The EKOB was subsequently affected by the Paleo-Tethys orogeny, which performed a key role in the generation of Permian–Triassic granitic magmatism (Yang et al., 1996). The Paleozoic tectonic evolution of the EKOB has been the focus of much research (Zhu C B et al., 2018; Liu et al., 2012; Zhang et al., 2010; Chen et al., 2008; Zhao et al., 2008; Li et al., 2006; Zhu Y H et al., 2006, 2005; Pan et al., 1996), although uncertainties remain. For example, Mo et al. (2007) put forward that subduction of the Proto-Tethys continued until the Late Ordovician, while Dong et al. (2017) considered that the Proto-Tethys Ocean has closed during

*Corresponding author: 691836152@qq.com

Manuscript received November 13, 2017.
Manuscript accepted May 22, 2018.

the Devonian. Neither view can emphasize the post-collision magmatism, while the granites and mafic-ultramafic complexes associated with post-collision extension can provide an effective method to deal with these contradictions.

The Maxingdawannan area in the Qimantagh region records the early tectonic evolution of the region and contains voluminous magmatic rocks. Therefore, an understanding of the geology of the area is vital in elucidating the tectonic evolution of the EKOB. Although some detailed studies of the Qimantagh region have been undertaken (Feng et al., 2012; Wang et al., 2012, 2009; Cui et al., 2011; Ma et al., 2010; Liu et al., 2006; Lu et al., 2006; Tan et al., 2004; Shen et al., 1999), its Paleozoic evolution remains unclear. Here we report new data for monzogranites and mafic-ultramafic complexes of the Maxingdawannan area, with the aim of establishing an evolutionary model of Early Devonian magmatism in the EKOB and further constraining the tectonic evolution of the EKOB.

1 GEOLOGICAL BACKGROUND AND SAMPLE DESCRIPTION

The EKOB is situated in the north section of Tibetan Plateau (Ju et al., 2017; Mo et al., 2007), bordered by the Qaidam Basin to the north and the Songpan-Ganzi Basin to the south (Fig. 1), extending 1 500 km from east to west and south-north of 50–200 km (Yang et al., 1996; Jiang et al., 1992). Sun et al. (2009) regarded the EKOB as a collage of blocks that experienced multiple stages of orogeny and accumulated northward to the Qaidam Block. Major E-W-trending faults delineate several belts, which from north to south are the Caledonian back-arc rift belt (north EKOB), the basement uplifted and granite belt (middle EKOB), and the composite collage belt (south EKOB)(Fig. 1; Sun et al., 2009). The northern EKOB comprises mainly basic volcanic rock that is locally overlain by Devonian sedimentary molasse, and the middle EKOB is characterized by intense granitic magmatism that covers an area of ~48 400 km^2. In the southern EKOB, exposed strata range from Paleoproterozoic to Triassic in age (Jiang et al., 1992), are generally intensely deformed, and are overlain by extensive Triassic strata. Sun et al. (2009) considered the marine basic volcanic rocks of the Mesoproterozoic Anbaogou Group to constitute an "Ocean Basalt Plateau". The middle and northern EKOB are located at the northern end of the middle Kunlun fault, and consist of a Paleoproterozoic crystalline basement (Jinshuikou Group). The Meso-Neoproterozoic southern EKOB comprises an oceanic plateau and a belt of tectono-stratigraphic terranes.

The study area is located in the middle EKOB (Fig. 1) 91°27′39″E–91°29′41″E and 36°55′23″N–36°58′01″N. Quaternary sediments are mainly exposed strata (Fig. 2). Northwest-southeast- and NE-SW-trending faults dominate the area. The NW-SE faults are strike-slip faults. Intrusive rocks are widespread and are dominated by monzogranite, granodiorite and diorite, as well as mafic-ultramafic complexes. The monzogranites are mainly Mesozoic and Paleozoic in age, and exposed area is ~6 km^2. The Mesozoic monzogranites occur in the northwestern part of the area, while the Paleozoic monzogranites occur in the eastern and middle parts. The granodiorites and diorites are found in the southwest and central parts of the area, respectively. The mafic-ultramafic complexes occur in the southern end of the district, where they outcrop over an area of ~0.73 km^2. Dikes, including granite porphyry, diorite and gabbro dikes, are also present in the area (Fig. 2).

The samples used for study were gained from outcrops in the southern and eastern Maxingdawannan area (Fig. 2). The monzogranites, collected from 36°55′56″N, 91°29′45″E (Figs. 2, 3a, 3c), are pale red, medium- and coarse-grained, massive and contain quartz (~35%), plagioclase (~27%), orthoclase (~30%), biotite (~5%), and minor zircon and titanite (~3%) (Figs. 4a, 4b). Samples from mafic-ultramafic complexes, collected at 36°55′43″N, 91°29′09″E (Figs. 2, 3b), are olivine gabbros and olivine pyroxenites. The olivine gabbros are pale-grey, fine- to medium-grained, massive, and contain plagioclase (~40%), clinopyroxene (~30%), olivine (~25%), and minor talc and biotite (~5%)(Figs. 3d, 4c). The olivine pyroxenites are dark-grey, fine- to medium-grained, massive, and contain clinopyroxene (~65%), olivine (~25%), plagioclase (~5%), and minor talc and biotite (~5%) (Figs. 3e, 4d). Early crystallized clinopyroxene was later transformed into talc by autometamorphism.

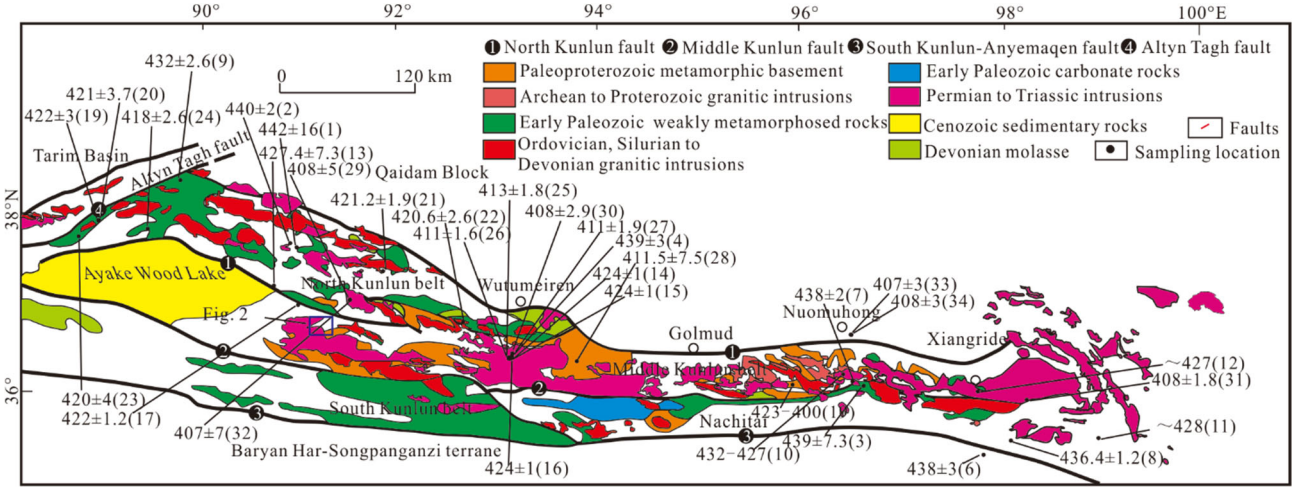

Figure 1. Geological map showing the regional structure of the east Kunlun orogenic belt.

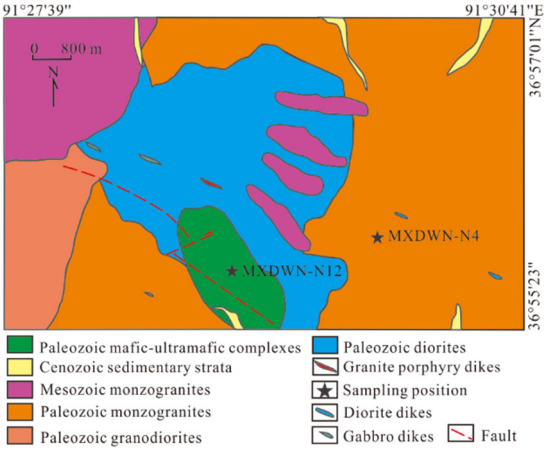

Figure 2. Geological map of the Maxingdawannan area.

2 ANALYTICAL METHODS

2.1 U-Pb Zircon Geochronology

Zircons were separated and extracted at the Langfang Regional Geological Survey, Hebei Province, China, according to the standard procedures. All zircons were examined carefully and their internal structures were revealed by cathodoluminescence (CL) images. Zircon U-Pb isotope analysis were implemented at the Yanduzhongshi Geological Analysis Laboratories, Beijing, China, following the method of Yuan et al. (2004), corrected method seen Andersen (2002). Isotopic data were calculated by the ICP-MS-DATECAL program (Liu Z Q et al., 2011; Liu Z X et al., 2008). Age calculations and generate concordia plots used Isoplot program (Ludwig, 2003). These data are listed in Table S1.

2.2 Whole-Rock Geochemistry

Whole-rock samples were performed in the Yanduzhongshi Geological Analysis Laboratories Ltd., Beijing, China. After removing altered surfaces, fresh samples were chosen and then grind to less than 200 mesh (0.520 0±0.000 1 g) for analysis. Sample powders were performing V8C automatic fusion machine procedure. The precision of major and trace elements are better than 1% and 5%, respectively. These data are shown in Table S2.

2.3 Zircon Hf Isotopes

Zircon Hf isotope analyses were carried out using a New-Wave UP213 laser system attached to a Neptune multi-collector ICP-MS, at the Institute of Mineral Resources, Chinese Academy of Geological Sciences, Beijing, China. The spot size of instrument is 55 μm. Analytical methods and process, data acquisition techniques see Guo et al. (2012) and Wu et al. (2006). Data are presented in Table S3.

3 RESULTS

3.1 U-Pb Zircon Geochronology

3.1.1 Monzogranites

Zircons from monzogranite sample MXDWN-16-DB-N4 are 100–150 μm long with aspect ratios of 1 : 1.5 to 1 : 3, and exhibit oscillatory zoning (Fig. 5). They have variable Th (58 ppm–249 ppm) and U (139 ppm–599 ppm) contents, with Th/U ratios of 0.34–0.79 (Table S1), consistent with a magmatic origin (Corfu et al., 2003; Hoskin and Schaltegger, 2003). The 24 analyses yield a mean age of 399±1 Ma (MSWD=1.07; Fig. 6a), interpreted as the crystallisation age of MXDWN monzogranites.

3.1.2 Mafic-ultramafic complexes

Cathodoluminescence images reveal that the zircon crystals from a gabbro sample (MXDWN-16-DB-N12) are mostly subhedral with noinherited cores. Most crystals are stubby prisms or subrounded with aspect ratios of 1 : 1.5 to 1 : 2.5 (Fig. 5). The samples have variable Th (384 ppm–2 191 ppm) and U (431 ppm–2 109 ppm) contents, and Th/U ratios of 0.54–1.4, which, together with internal textures, indicate a magmatic origin (Corfu et al., 2003; Hoskin and Schaltegger, 2003). Thirty-two analyses yielded ages of 402–393 Ma, with a weighted-mean age of 397±1 Ma (MSWD=0.42; Fig. 6b), interpreted as the crystallization age of MXDWN gabbros.

Figure 3. Photographs showing (a) outcrop of monzogranites in the Maxingdawannan area, (b) outcrop of mafic-ultramafic complexes in the Maxingdawannan area, (c) hand specimen of monzogranites, (d) and (e) hand specimen of mafic-ultramafic complexes, (d) olivine gabbro, (e) olivine pyroxenite.

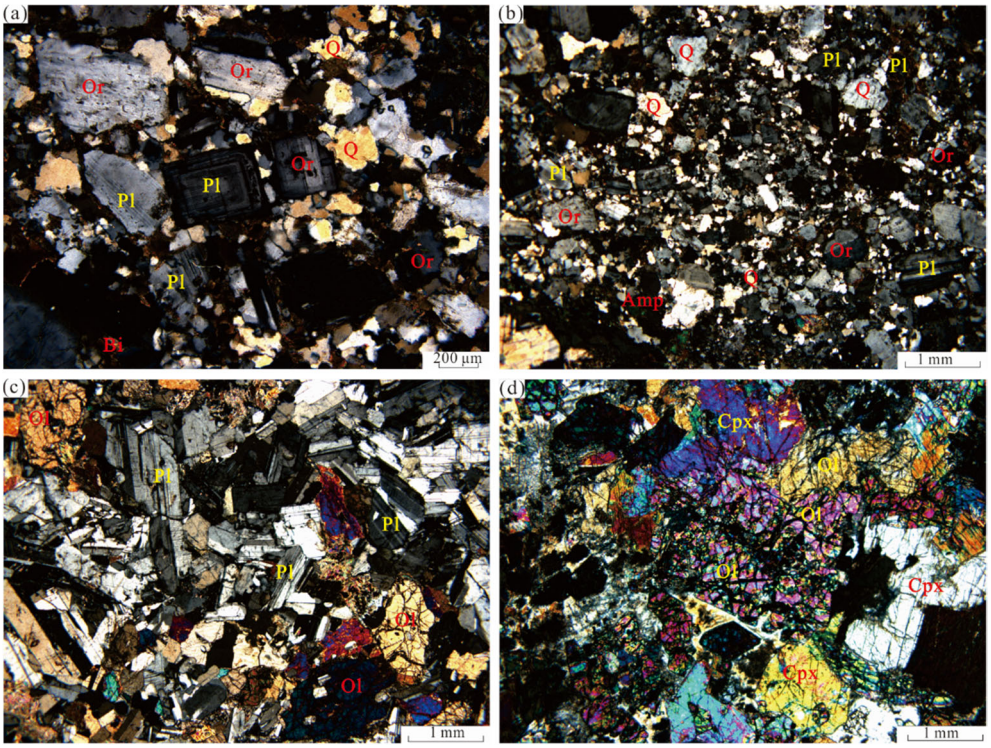

Figure 4. Photomicrographs showing monzogranites and mafic-ultramafic complexes of the Maxingdawannan area (crossed-polarized light). (a), (b) Monzogranite; (c) troctolite; (d) olivine pyroxenolite. Pl. Plagioclase; Q. quartz; Cpx. clinopyroxene; Or. orthoclase; Ol. olivine; Bi. biotite.

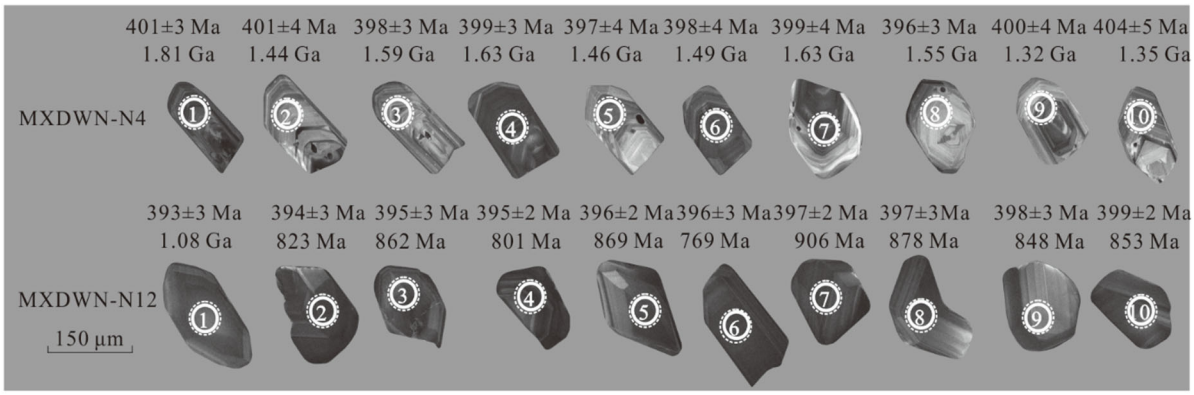

Figure 5. Cathodoluminescence (CL) images of zircons selected for analysis from the Early Devonian rocks of the study area. The numbers on these images indicate individual analysis spots, and the values below the images show zircon ages and their T_{DM} (Hf) ages.

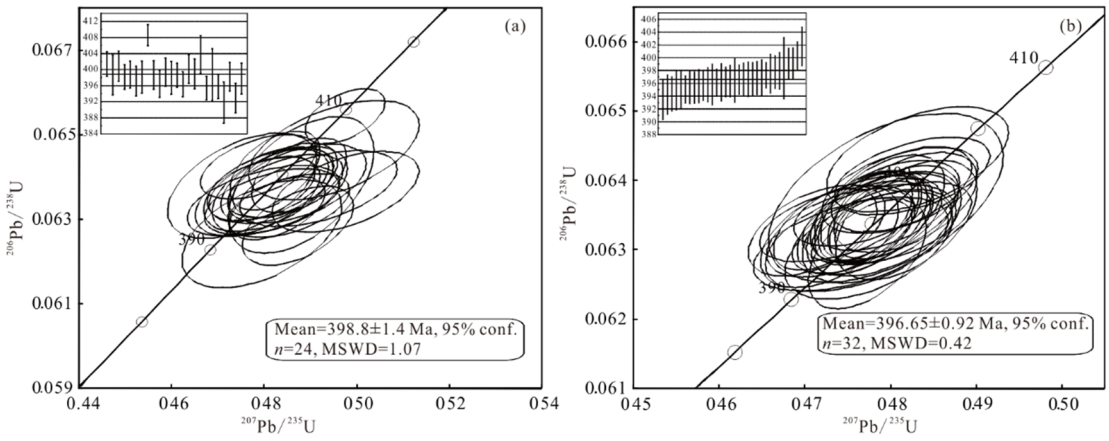

Figure 6. U-Pb isotope concordia diagrams for analyzed zircons from (a) monzogranite and (b) gabbro (insets show weighted mean age diagrams).

3.2 Whole-Rock Geochemistry

3.2.1 Monzogranites

The monzogranites contain 64.8 wt.%–66.8 wt.% SiO_2, 14.1 wt.%–14.6 wt.% Al_2O_3, 2.56 wt.%–3.28 wt.% Na_2O, 4.20 wt.%–5.95 wt.% K_2O (Na_2O/K_2O=0.43–0.78), 1.97 wt.%–2.76 wt.% CaO, 0.76 wt.%–0.81 wt.% TiO_2, 4.59 wt.%–5.22 wt.% TFeO, 0.92 wt.%–1.13 wt.% MgO, and $Mg^{\#}$=28.0–30.0 ($Mg^{\#}$=100×MgO/(MgO+TFeO)). The monzogranites are related to quartz monzonite series in the TAS diagram (Fig. 7a), and within the shoshonite series in the K_2O vs. SiO_2 diagram (Fig. 7b), with A/CNK ratios of 0.94–1.06. The samples have right-declining REE patterns (Fig. 8a) with $(La/Yb)_N$ ratios of 3.67–6.94 and negative Eu anomalies (Eu/Eu*=0.36–0.48). Primitive-mantle-normalized variation patterns (Fig. 8b) indicate Rb, U and Sr enrichment and strong Nb, Ta and Ti depletion.

3.2.2 Mafic-ultramafic complexes

The loss-on-ignition (LOI) values of 1 wt.%–5 wt.% indicate significant weathering and/or alteration of the olivine gabbros and olivine pyroxenites (Li et al., 2018). The olivine gabbros contain 47.3 wt.%–52.0 wt.% SiO_2, 16.1 wt.%–21.3 wt.% Al_2O_3, 0.32 wt.%–3.15 wt.% TiO_2, 6.07 wt.%–11.82 wt.% TFe_2O_3, 7.54 wt.%–12.7 wt.% CaO, 1.80 wt.%–4.59 wt.% Na_2O+K_2O, 5.00 wt.%–8.87 wt.% MgO, and $Mg^{\#}$=46.88–77.33. The olivine pyroxenites contain 41.3 wt.%–42.9 wt.% SiO_2, 7.26 wt.%–9.13 wt.% Al_2O_3, 0.45 wt.%–0.82 wt.% TiO_2, 11.7 wt.%–12.7 wt.% TFeO, 4.96 wt.%–6.05 wt.% CaO, 0.99 wt.%–1.38 wt.% Na_2O+K_2O, 23.0 wt.%–24.7 wt.% MgO, and $Mg^{\#}$=79.5–81.5. The LREE contents and $(La/Yb)_N$ ratios of the olivine gabbros are 25.20 ppm–73.57 ppm and 4.44–5.03, respectively, and those of the olivine pyroxenites are 17.39 ppm–35.52 ppm and 2.96–3.18, respectively (Fig. 8c). Both rock types are depleted in Nb and Ta (Fig. 8d) and show weak Eu anomalies (Eu/Eu*=0.85–1.16; Fig. 8c; Sun and McDonough, 1989).

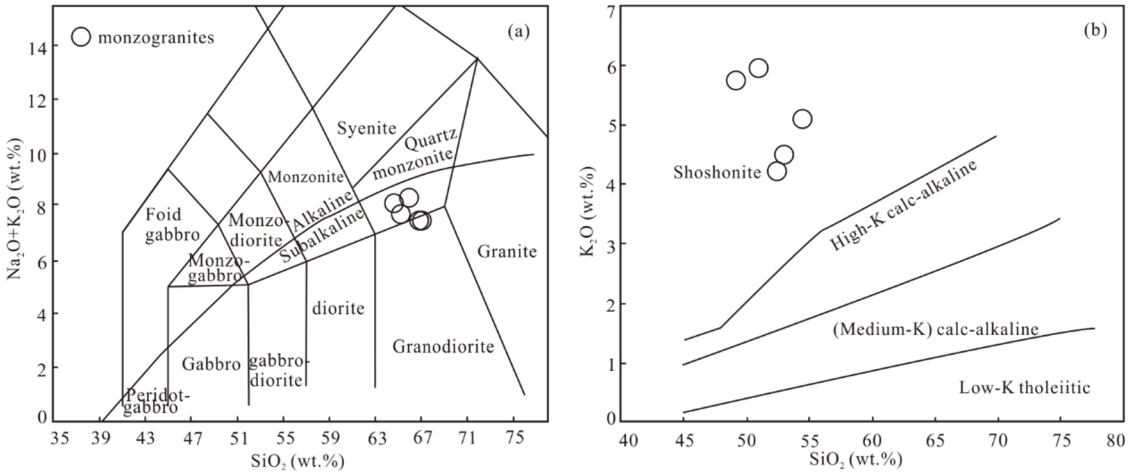

Figure 7. (a) SiO_2-(Na_2O+K_2O) diagram (Irvine and Baragar, 1971), and (b) SiO_2-K_2O diagram (Peccerillo and Taylor, 1976) of the Maxingdawannan monzogranite.

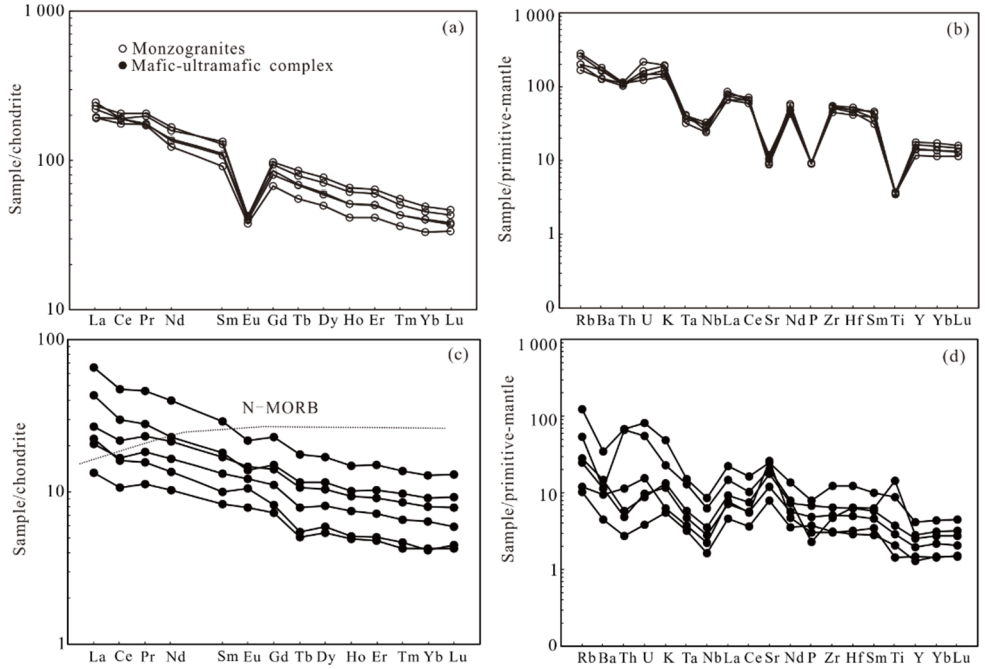

Figure 8. Trace elements characteristics of monzogranite showing (a) chondrite-normalized REE patterns, (b) primitive-mantle-normalized trace elements abundances (Sun and McDonough, 1989), and mafic-ultramafic complexes (c) and (d) of the Maxingdawannan monzogranite.

3.3 Zircon Hf Isotopes

Fifteen spot analyses were gained from the MXDWN monzogranite samples, yielding $^{176}Yb/^{177}Hf$ ratios of 0.016 555–0.039 955 and $^{176}Lu/^{177}Hf$ ratios of 0.000 584–0.001 388. $^{176}Hf/^{177}Hf$ ratios are ranging from 0.282 343 to 0.282 560, which corresponds to $\varepsilon_{Hf}(t)$ values of -6.68 to 1.11 (weighted mean -1.99; Fig. 9). T_{DM2} model ages vary from 1.32 to 1.81 Ga (weighted mean 1.52 Ga; Table S3).

Twelve spot analyses on MXDWN gabbro samples yielding $^{176}Yb/^{177}Hf$ ratios of 0.019 772–0.030 968 and $^{176}Lu/^{177}Hf$ ratios of 0.000 680–0.001 117. $^{176}Hf/^{177}Hf$ ratios are 0.282 480–0.282 711 with $\varepsilon_{Hf}(t)$ values of -1.81 to 6.29 (Fig. 9). T_{DM1} model ages are 1 087–769 Ma (weighted-mean 865 Ma; Table S3).

4 DISCUSSION

4.1 Early Devonian Magmatism in the EKOB

There is a general consensus that intrusive rocks in the EKOB were mostly emplaced in Early Paleozoic and Early Mesozoic (Dai et al., 2013; Feng C Y et al., 2012, 2010; Cao et al., 2011; Cui et al., 2011; Chen et al., 2006). However, voluminous intrusive rocks within the Maxingdawannan area have not yet be precisely dated. Based on rock associations and lithostratigraphic relationships with surrounding rocks, it was initially identificated as monzogranites and mafic-ultramafic complexes by the China Aero Geophysical Survey and Remote Sensing Center (AGRS) during regional geological mapping. This study firstly provides precise U-Pb dating of the monzogranites and mafic-ultramafic complexes in the Maxingdawannan area.

The ages of the Early Paleozoic Maxingdawannan monzogranites and mafic-ultramafic complexes (399 and 397 Ma, respectively) are consistent with those of Early Paleozoic magmatic activity in other parts of the EKOB (Fig. 10; Wang et al., 2013; Liu et al., 2012; Chen et al., 2006). For example, ~407 and 406 Ma granodiorites and gabbros are found in the Yuejinshan area (Liu et al., 2012), ~406 Ma websterite and ~405 Ma gabbronorite in the Xiarihamu (Song et al., 2016), ~391 Ma syenogranites occur in the Xiarihamu area (Wang et al., 2014, 2013), and ~403 and 394 Ma gabbros and syenogranites are present in the Kayakedengtage area (Chen et al., 2006). The new U-Pb ages for the Maxingdawannan area, together with previously published data, indicate a widespread Early Devonian igneous event in the EKOB.

4.2 Magma Sources and Petrogenesis

4.2.1 Petrogenesis

4.2.1.1 Monzogranites

The geochemical data of the Early Devonian monzogranites collected from the Maxingdawannan area can be utilized to trace their magma sources. The monzogranites have elevated SiO_2, Al_2O_3, and alkali element concentrations. In contrast, the concentrations of TFe_2O_3, MgO ($Mg^{\#}$=28.04–30.00), P_2O_5, and TiO_2 are relatively low. The monogranites have high Zr+Nb+Ce+Y contents (>698 ppm) and 10 000 Ga/Al ratios (>2.46), consistent with A-type granites (Whalen et al., 1987). In the $(Zr+Nb+Ce+Y)\times10^{-6}$ vs. $(K_2O+NaO)/CaO$, $(Zr+Nb+Ce+Y)\times10^{-6}$ vs. TFeO/MgO, 10 000Ga/Al vs. $(K_2O+NaO)/CaO$, and 10 000Ga/Al vs. TFeO/MgO diagrams (Fig. 11; Whalen et al., 1987), most samples plot in the A-type granite field. Furthermore, in the Nb vs. Y vs. Ce and Y/Nb vs. Rb/Nb diagrams (Fig. 12), the Maxingdawannan A-type granites plot in the A_2 subgroup, indicating their formation in a post-collisional setting. Zircon saturation thermometry (Watson and Harrison, 1983; Watson, 1979) can be used to estimate the temperatures of felsic magma. The zircon saturation temperature (827–865 °C; mean 842 °C) is close to the A-type granite temperature of 839 °C (Chen et al., 2018).

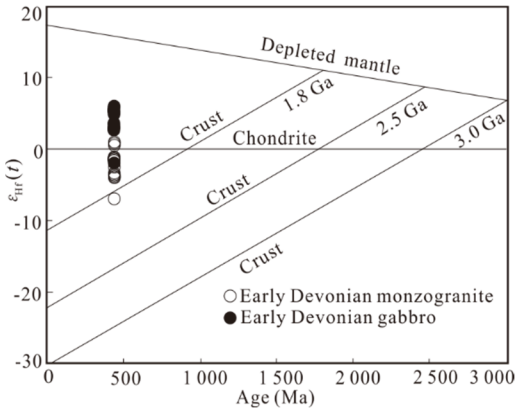

Figure 9. Zircon Hf isotopic features for the Early Devonian intrusive rocks in Maxingdawannan area.

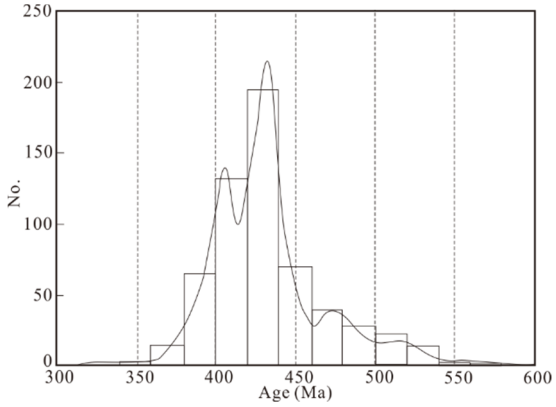

Figure 10. Probability curve of ages for magmatic zircons from the east Kunlun orogenic belt.

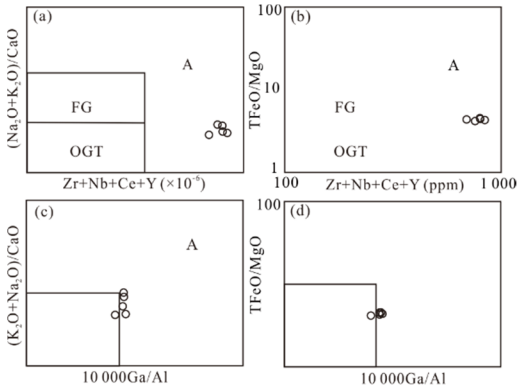

Figure 11. (a) $Zr+Nb+Ce+Y(\times10^{-6})$-$(K_2O+Na_2O)/CaO$ diagram; (b) $Zr+Nb+Ce+Y(\times10^{-6})$-TFeO/MgO diagram; (c) 10 000Ga/Al-$(Na_2O+K_2O)/CaO$ diagram and (d) 10 000Ga/Al-TFeO/MgO diagram (after Whalen et al., 1987) of the Maxingdawannan monzogranite. FG. Fractionated felsic granites; OGT. unfractionated M-, I-and S-type granites; A. A-type granites.

4.2.1.2 Mafic-ultramafic complexes

It is unavoidable that mantle-sourced magma will undergo contamination before the magma was emplaced. LILEs in enrichment and HFSEs in depletion, combined with the REE patterns of the Maxingdawannan complexes, unlike those of N-MORB originated from asthenospheric mantle source (Fig. 8c). Some elements ratios would not be affected during fractional crystallization and partial melting, due to the similar distribution coefficient (MacDonald, 2001; Campbell and Griffiths, 1993). Among these elements and their ratios (e.g., K_2O/P_2O_5, Ce/Pb, Ta/Yb, Nb/Ta and Th/Yb), their covariant relationships can efficiently detect whether crustal components were incorporated into the magma. Positive correlation between the Th/Yb-Nb/La, and La/Yb-Ce/Yb are indicated in Figs. 13a, 13b. Nb/U and Ce/Pb ratios will remain constant during magmatic evolution; accordingly, implying their origin. Hofmann (1988) suggest that Nb/U ratios of MORB and OIB are 47±10. By comparison, Maxingdawannan mafic-ultramafic complexes have Nb/U ratio range from 3.57 to 14.62, which is close to the mean value of the net continental crust (~9.7; Campbell, 2002). In addition, Ce/Pb ratio in the mantle is 25±5, as for the continental crust is less than 15 (Furman et al., 2004). The Maxingdawannan mafic-ultramafic complexes have Ce/Pb ratio range from 1.24 to 3.52 (mean of 2.35), suggesting that incorporated significant crustal material. $(La/Nb)_{PM}$ and $(Th/Ta)_{PM}$ value for the upper and lower crust are markedly different, meaning these trace element ratios can be utilized to ascertain the contaminants (Neal et al., 2002). In Fig. 14, samples either plot near the upper crust or near the lower crust, implying that both the upper and lower crust were the sources of contamination.

4.2.2 Magma sources

4.2.2.1 Monzogranites

A-type granites commonly originate from partial melting of felsic crust under low pressure and have negative Eu anomalies and relatively flat HREE patterns. Their Rb/Sr and Rb/Nb values differ from those of coeval mafic-ultramafic complexes, and they contain no mafic enclaves. Based on field and microscopic observations and geochemical analyses, we consider that the Maxingdawannan A-type granites are in this category. Moreover, the Rb/Sr ratios (0.50–0.86) and Rb/Nb ratios (6.0–7.6) of monzogranites are higher than the mean values for global continental crust (0.32 and 4.5, respectively), which also supports a crustal origin for the magmas. Besides, the monzogranites are LILEs in enrichment and HFSEs in depletion, suggesting that these magma was originated from partial melting of the crust (Wu et al., 2000). Depletions in Ti, Nb and Ta indicate that the source for the magma are contained residual ilmenite, rutile and titanite (McKenzie, 1989; Sun and McDonough, 1989). The negative Eu anomalies indicate that these magmas either fractionated plagioclase or were derived from a source containing residual plagioclase.

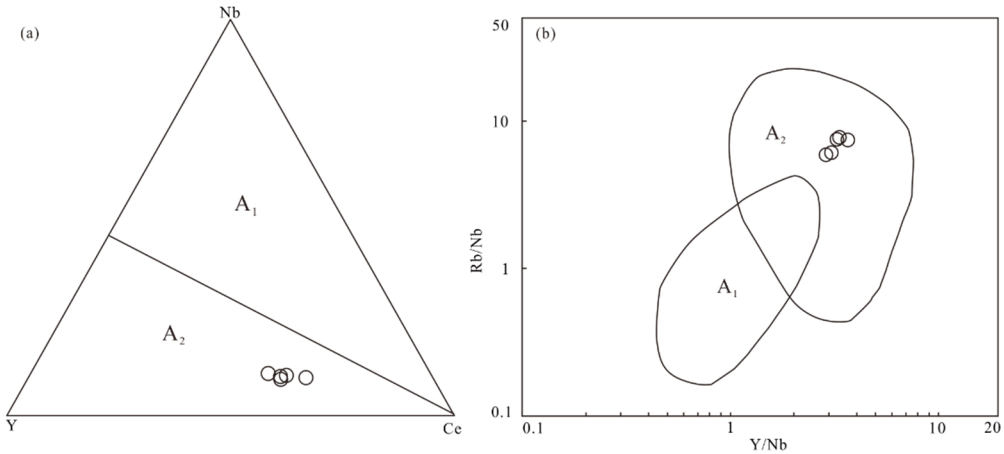

Figure 12. (a) Nb-Y-Ce diagram, and (b) Y/Nb-Rb/Nb diagram of the Maxingdawannan monzogranite. Modified after Eby (1992). A1. A1-type granites; A2. A2-type granites.

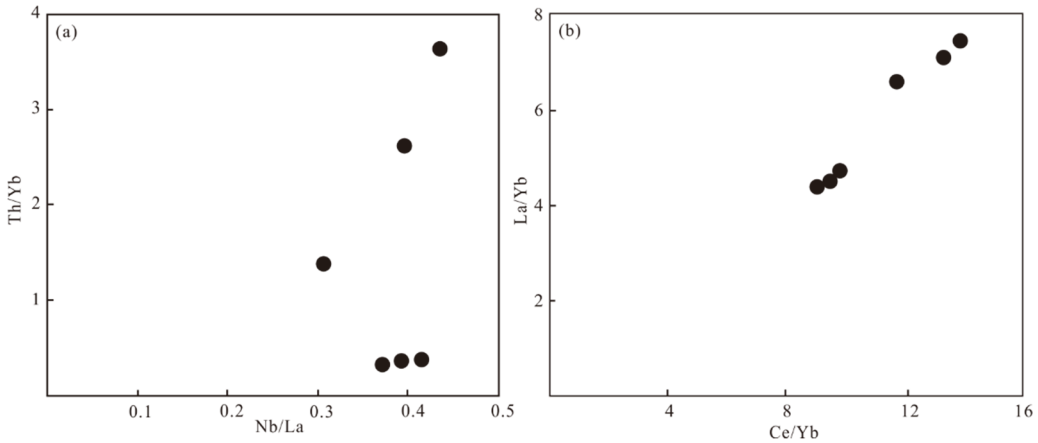

Figure 13. Plots of selected trace element for checking contamination of the Maxingdawannan mafic-ultramafic complexes.

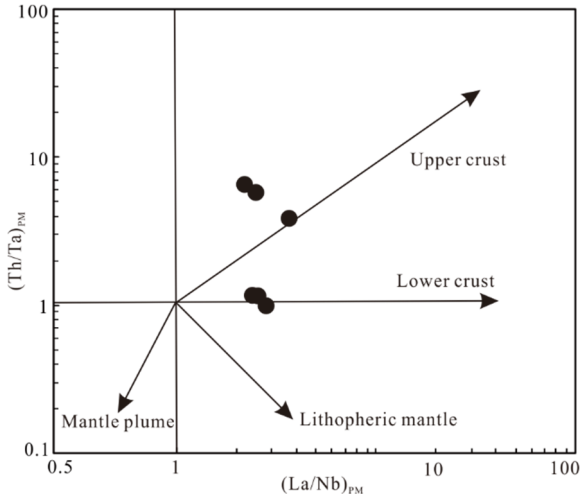

Figure 14. $(La/Nb)_{PM}$ vs. $(Th/Ta)_{PM}$ diagrams for Maxingdawannan mafic-ultramafic complexes (after Neal et al., 2002).

The zircons from the monzogranites have $\varepsilon_{Hf}(t)$ values of -6.68 to 1.11 (mean value of -1.99; Table S3) and $^{176}Hf/^{177}Hf$ ratios of 0.282 343 to 0.282 560, reflecting that the zircons didn't crystallize from a homogeneous magma (Andersen et al., 2007). Negative $\varepsilon_{Hf}(t)$ values are consistent with crustal melt, while positive values may indicate mantle components or juvenile crust (Wang et al., 2014, 2013). The older T_{DM2} ages of ca. 1.81 Ga for the monzogranites resemble the formation age of the Baishahe Group (Wang et al., 2007), indicating that older continental crust materials might do duty for the principal source. The positive Hf for monzogranites suggest that the source might have incorporated into a high-proportioned juvenile materials. In conclusion, we conclude that the monzogranites are probably originated from partial melting of ancient lower crust during the Paleo-Mesoproterozoic, including juvenile crustal materials.

4.2.1.2 Mafic-ultramafic complexes

The $\varepsilon_{Hf}(t)$ values of zircons are intermediate between those of chondrites and depleted mantle (Fig. 9), implying the gabbros were mainly associated with partial melting of depleted mantle. Except for two samples, Zr/Nb and Sm/Nd ratios are 22.31–29.74 and ~0.26, respectively, similar to MORB values (10–60 and ~0.32, Davidson, 1996; Anderson, 1994). But Hf model ages T_{DM1} (1 087–769 Ma) of the zircons are much older. If the primitive magma of the zircons came from depleted mantle, Hf model ages would represent the time of separation of zircon from source. Under the circumstances, the crystallization ages (397 Ma) should be comparably equal to the Hf model ages (Wu et al., 2007, 2004). Therefore, we consider that the enriched materials have contaminated the magma source.

Nb/U ratios are generally defined to reflect the mantle source characteristics, on account of uniform partition coefficient during magmatic crystallization process. MORB and OIB have Nb/U ratios of ~50 (McDonough and Sun, 1995) and continental upper crust ~9 (Rudnick and Fountain, 1995), but arc volcanic rocks have lower ratios of 0.3–9 (Chung et al., 2001). If mantle rocks are generated by contamination of the crust materials, Nb/U ratios should be between ~9 and ~50. We've found that three rocks have Nb/U ratios of 9.97–14.64, this may be the result of contamination. The other three rocks have lower Nb/U ratios (3.57–4.93) than those of continental upper crust but fall into the range of arc volcanic rocks. This signifies that these rocks aren't formed by contamination, but stemmed from a metasomatic mantle source.

Previous researches have suggested that the bulk of fluid-soluble elements would be affected by an influx of water from the subducting plate in the mantle wedge, but HFSEs are relatively depleted (Regelous et al., 1997). Thus, the LILEs in enrichment and HFSEs in depletion are due to the metasomatism of the mantle wedge (Peng et al., 2016), as observations of the Maxingdawannan mafic-ultramafic complexes. In the Th/Yb vs. Nb/Yb diagram, the mafic-ultramafic complexes, plotting close to the volcanic arc array (Fig. 15a), which reflects the input of subduction materials (Pearce and Peate, 1995). Ba/Th and Th/Nb ratios can effectively distinguish between slab fluid and sediment melts. Maxingdawannan mafic-ultramafic complexes have Th/Nb and Th/Yb ratios of 0.20–1.27 and 0.32–3.64, respectively. Figure 15b shows that large volumes of fluids were injected into the source region of the parental magmas (Hanyu et al., 2006). In conclusion, we consider that the Maxingdawannan mafic-ultramafic complexes are resulted from magma originated from a depleted mantle source, which had previously been metasomatized by slab fluids.

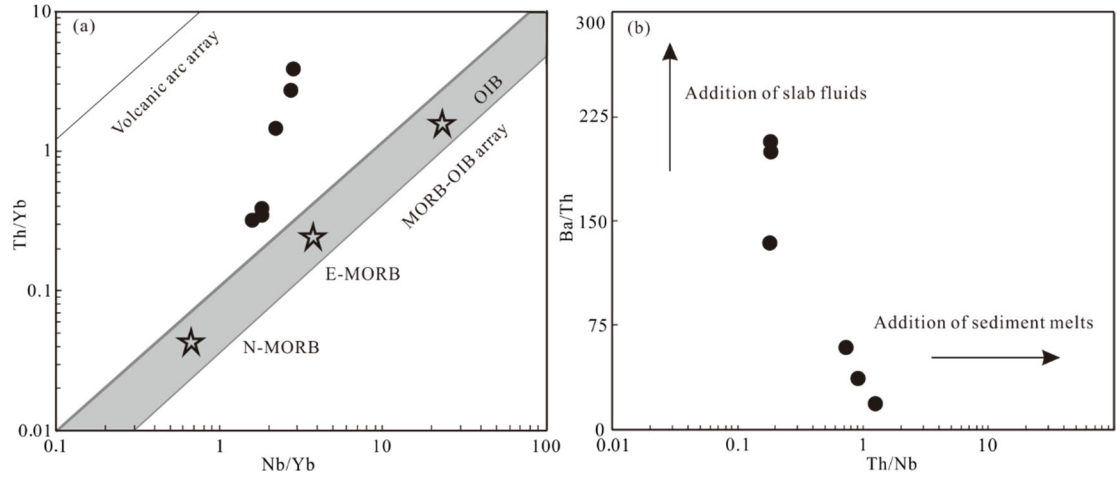

Figure 15. (a) Nb/Yb vs. Th/Yb, (b) Th/Nb vs. Ba/Th diagrams of the Maxingdawannan mafic-ultramafic complexes (after Hanyu et al., 2006; Pearce and Peate, 1995).

4.3 Tectonic Implications

4.3.1 Post-collision magmatism in the EKOB

A-type granites are normally considered to form in an extension setting (Eby, 1992; Whalen et al., 1987), with A_2-type granites representing a post-orogenic setting. Mafic-ultramafic complexes are also considered A-type granites. Granites in the western EKOB have received little attention, and study of their petrogenesis may help constrain the dynamical evolution of the Proto-Tethys Ocean. As mentioned above, we suggest that Maxingdawannan monzogranites have a A_2-type origin. The Maxingdawannan A_2-type granites (399 Ma) and associated mafic-ultramafic complexes (397 Ma) indicate the onset of an Early Devonian post-collision setting in the EKOB.

Many granitic rocks in the EKOB have been generated in a post-collision extensional setting (419.0±1.7 Ma, Yan et al., 2016; 420.6±2.6 Ma, Hao et al., 2015; 407±1.7 Ma, Liu et al., 2012; 432 Ma, Gao et al., 2010; 420±4 Ma, Hao et al., 2003). Massive magmatic Ni-(Cu) sulfide deposits linked with mafic-ultramafic complexes (424–394 Ma; Peng et al., 2016; Song et al., 2016; Wang et al., 2014; Li et al., 2012) and 391 Ma post-orogenic A_2-type granites in the Xiarihamu area (Wang et al., 2013) are indicative of strong extension. The ages of the Maxingdawannan monzogranites and associated mafic-ultramafic complexes overlap those of the Xiarihamu Ni-(Cu) Deposit (394–424 Ma; Peng et al., 2016; Song et al., 2016; Wang et al., 2014; Li et al., 2012), which is consistent with post-collisional extension. Given the facts above, the authors inclined to support the view of Dong et al. (2017), that is, EKOB was in the post-collisional setting during the Early Devonian.

4.3.2 Regional geodynamics

Systematic studies of the opening and expansion of the Early Paleozoic oceans related to the rifting and prolonged break-up of the Rodinia supercontinent at 860–570 Ma in the EKOB were presented by Feng J Y et al. (2010), Li et al. (2008), Lu (2001) and Yang et al. (1996). Early Paleozoic ophiolites represent Proto-Tethyan oceanic crust along the central Kunlun suture (Liu et al., 2011; Yang et al., 1996) that formed mainly at 525–509 Ma (Kong et al., 2017; Liu et al., 2011; Lu, 2002). Subsequently, along the middle Kunlun fault, the Proto-Tethys oceanic lithosphere began subducting to the north, meaning that the southern margin of Qaidam Block switched from passive to active property. A series of volcanic events may have occurred along the middle Kunlun active epi-continental arc in this period (Liu et al., 2013a, b; Cui et al., 2011; Chen F et al., 2002; Chen N S et al., 2002). Gabbro from Qingshuiquan area (452±5 Ma; Sang et al., 2016), basalt from the Kuangou-Xiaolangyashan area (440±2 Ma; Wang et al., 2012) and basalt from Qimantagh area (439±1.2 Ma; Li et al., 2008) were the products of northward subduction of Proto-Tethys oceanic lithosphere. Along the middle Kunlun suture zone, these mafic plutons and dikes may represent the earliest stage of magmatism relevant to the Early Paleozoic subduction of oceanic crust (Peng et al., 2016; Liu et al., 2013a, b). Monzogranite and rapakivi were formed in continental collision setting that yield crystallization ages of 430.8±1.7 and 428.5±2.2 Ma in the EKOB, respectively (Cao et al., 2011). Moreover, eclogites with ages of ~428 Ma were formed in the course of closure of the Proto-Tethys Ocean (Meng et al., 2013). Furthermore, the deposition of molasse sediments of Maoniushan Formation (423–400 Ma; Lu, 2002, 2001) indicate that subduction did not continue to Devonian. Collectively, the ages of these rocks indicate that continent-continent collision, including post-collision extension and closure of the Proto-Tethys, finished at ~430 Ma.

Northward subduction of the Proto-Tethys oceanic plate was resulted in metasomatism and enrichment of the subcontinental lithospheric mantle by slab fluids during the Early Paleozoic. At the same time, the Proto-Tethys oceanic lithosphere was accreted to the Qaidam Block and then the closure of Proto-Tethys Ocean. By reason of its great thickness (25–35 km), subduction of the Proto-Tethys oceanic lithosphere was impeded, whereas the previously subducted oceanic crust continued sinking into the mantle. Thus, the subducting slab broke due to the asymmetrical tensional forces, resulting in the formation of a slab window. Asthenospheric mantle upwells through the slab window and then partial melting. Overlying enriched lithospheric mantle would be incorporated into the primary magmas during their uprise. Fractional crystallisation plus crustal contamination was resulted in S saturation and sulphide liquation, and then magmatic differentiation. These differentiated magmas ascended into the crust under buoyancy, forming the mafic-ultramafic complexes. Subsequently, the overlying felsic crust was heated by upwelling and melting of the asthenosphere, resulting in partial melting of the felsic crust at low pressure and formation of the monzogranites (Fig. 16).

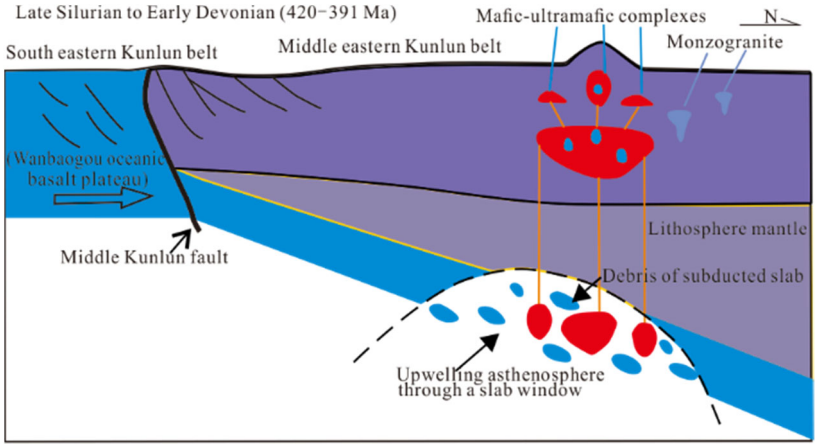

Figure 16. Geodynamic sketch map of monzogranite and mafic-ultramafic complexes, modified after Wang et al. (2014a).

5 CONCLUSIONS

(1) U-Pb zircon dating shows that the monzogranites (398.8±1.4 Ma) and mafic-ultramafic complexes (396.65±0.92 Ma) were formed during the Early Devonian.

(2) The monzogranites were probably generated by partial melting of ancient lower crust during the Paleo-Mesoproterozoic, involving juvenile crustal melt. The mafic-ultramafic complexes were probably originated from a depleted mantle source that had previously been modified by slab fluids. Crustal materials were incorporated into the primitive magmas during their ascent.

(3) The Early Devonian intrusions were associated with northward subduction of the Proto-Tethys oceanic lithosphere.

ACKNOWLEDGMENTS

We thank the staff of the Yanduzhongshi Geological Analysis Laboratories Ltd., Institute of Mineral Resources, Chinese Academy of Geological Sciences, for helping in the analysis. This work was supported by the National Natural Science Foundation of China (No. 41272093), and China Geological Survey (No. 12120114080901). The final publication is available at Springer via https://doi.org/10.1007/s12583-018-1203-8.

Electronic Supplementary Materials: Supplementary materials (Tables S1, S2, S3) are available in the online version of this article at https://doi.org/10.1007/s12583-018-1203-8.

REFERENCES CITED

Andersen, T., 2002. Correction of Common Lead in U-Pb Analyses That do not Report ^{204}Pb. *Chemical Geology*, 192(1/2): 59–79. https://doi.org/10.1016/s0009-2541(02)00195-x

Andersen, T., Griffin, W. L., Sylvester, A. G., 2007. Sveconorwegian Crustal Underplating in Southwestern Fennoscandia: LAM-ICPMS U-Pb and Lu-Hf Isotope Evidence from Granites and Gneisses in Telemark, Southern Norway. *Lithos*, 93(3/4): 273–287. https://doi.org/10.1016/j.lithos.2006.03.068

Anderson, D. L., 1994. Komatiites and Picrites: Evidence That the 'Plume' Source is Depleted. *Earth and Planetary Science Letters*, 128(3/4): 303–311. https://doi.org/10.1016/0012-821x(94)90152-x

Campbell, I. H., 2002. Implications of Nb/U, Th/U and Sm/Nd in Plume Magmas for the Relationship between Continental and Oceanic Crust Formation and the Development of the Depleted Mantle. *Geochimica et Cosmochimica Acta*, 66(9): 1651–1661. https://doi.org/10.1016/s0016-7037(01)00856-0

Campbell, I. H., Griffiths, R. W., 1993. The Evolution of the Mantle's Chemical Structure. *Lithos*, 30(3/4): 389–399. https://doi.org/10.1016/0024-4937(93)90047-g

Cao, S. T., Liu, X. K., Ma, Y. S., et al., 2011. The Discovery of Early Silurian Intrusive Rocks in Qimantage Area and Its Geological Significance. *Qinghai Sci. Technol.*, 5: 26–30 (in Chinese)

Chen, A. X., Zhou, D., Zhang, Q. K., et al., 2018. Age, Geochemistry, and Tectonic Implications of Dulaerqiao Granite, Inner Mongolia. *Journal of Earth Science*, 29(1): 78–92. https://doi.org/10.1007/s12583-017-0817-6

Chen, F., Satir, M., Ji, J., et al., 2002. Nd-Sr-Pb Isotopes of Tengchong Cenozoic Volcanic Rocks from Western Yunnan, China: Evidence for an Enriched-Mantle Source. *Journal of Asian Earth Sciences*, 21(1): 39–45. https://doi.org/10.1016/s1367-9120(02)00007-x

Chen, N. S., He, L., Sun, M., et al., 2002. Precise Timing of the Early Paleozoic Metamorphism and Thrust Deformation in the Eastern Kunlun Orogen. *Chinese Science Bulletin*, 47(13): 1130–1133 (in Chinese)

Chen, S. J., Li, R. S., Ji, W. H., et al., 2008. Carboniferous Period Lithofacies Character and Tectono-Paleogeography in Kunlun Orogenic Belt. *Journal of Earth Sciences and Environment*, 3: 221–233 (in Chinese with English Abstract)

Chen, X. H., Gehrels, G., Yin, A., et al., 2015. Geochemical and Nd-Sr-Pb-O Isotopic Constrains on Permo–Triassic Magmatism in Eastern Qaidam Basin, Northern Qinghai-Tibetan Plateau: Implications for the Evolution of the Paleo-Tethys. *Journal of Asian Earth Sciences*, 114: 674–692. https://doi.org/10.13039/501100004613

Chen, H. W., Luo, Z. H., Mo, X. X., et al., 2006. SHRIMP Ages of Kayakedengtage Complex in the East Kunlun Mountains and Their Geological Implications. *Acta Petrologica et Mineralogica*, 25(1): 25–32 (in Chinese with English Abstract)

Chung, S. L., Wang, K. L., Crawford, A. J., et al., 2001. High-Mg Potassic Rocks from Taiwan: Implications for the Genesis of Orogenic Potassic Lavas. *Lithos*, 59(4): 153–170. https://doi.org/10.1016/s0024-4937(01)00067-6

Corfu, F., Hanchar, J. M., Hoskin, P. W., et al., 2003. Atlas of Zircon Textures. *Reviews in Mineralogy and Geochemistry*, 53: 469–500

Cui, M. H., Meng, F. C., Wu, X. K., 2011. Early Ordovician Island Arc of Qimantagh Mountain, Eastern Kunlun: Evidences from Geochemistry, Sm-Nd Isotope and Geochronology of Intermediate-Basic Igneous Rocks. *Acta Petrologica Sinica*, 27: 3365–3379 (in Chinese with English Abstract)

Dai, J. G., Wang, C. S., Hourigan, J., et al., 2013. Multi-Stage Tectono-Magmatic Events of the Eastern Kunlun Range, Northern Tibet: Insights from U-Pb Geochronology and (U-Th)/He Thermochronology. *Tectonophysics*, 599: 97–106. https://doi.org/10.1016/j.tecto.2013.04.005

Davidson, J. P., 1996. Deciphering Mantle and Crustal Signatures in Subduction Zone Magmatism: Subduction Top to Bottom. *Geophysical Monograph Series*, 96: 251–262. https://doi.org/10.1029/GM096p0251

Deng, J., Wang, C. M., Bagas, L., et al., 2015. Cretaceous-Cenozoic Tectonic History of the Jiaojia Fault and Gold Mineralization in the Jiaodong Peninsula, China: Constraints from Zircon U-Pb, Illite K-Ar, and Apatite Fission Track Thermochronometry. *Mineralium Deposita*, 50(8): 987–1006. https://doi.org/10.1007/s00126-015-0584-1

Deng, J., Wang, C. M., Li, G. J., 2012. Style and Process of the Superimposed Mineralization in the Sanjiang Tethys. *Acta Petrologica Sinica*, 28: 1349–1361 (in Chinese with English Abstract)

Deng, J., Wang, Q. F., Li, G. J., et al., 2014a. Cenozoic Tectono-Magmatic and Metallogenic Processes in the Sanjiang Region, Southwestern China. *Earth-Science Reviews*, 138: 268–299. https://doi.org/10.1016/j.earscirev.2014.05.015

Deng, J., Wang, Q. F., Li, G. J., et al., 2014b. Tethys Tectonic Evolution and Its Bearing on the Distribution of Important Mineral Deposits in the Sanjiang Region, SW China. *Gondwana Research*, 26(2): 419–437. https://doi.org/10.1016/j.gr.2013.08.002

Dong, Y. P., He, D. F., Sun, S. S., et al., 2017. Subduction and Accretionary Tectonics of the East Kunlun Orogen, Western Segment of the Central China Orogenic System. *Earth-Science Reviews*, 186: 231–261. https://doi.org/10.1016/j.earscirev. 2017.12.006

Eby, G. N., 1992. Chemical Subdivision of the A-Type Granitoids: Petrogenetic and Tectonic Implications. *Geology*, 20(7): 641–644. https://doi.org/10.1130/0091-7613(1992)020<0641:csotat>2.3.co;2

Feng, C. Y., Li, D. S., Wu, Z. S., et al., 2010. Major Types, Time-Space Distribution and Metallogenesis of Polymetallic Deposits in the Qimantage Metallogenic Belt, Eastern Kunlun Area. *Northwestern Geology*, 43(4): 10–17 (in Chinese with English Abstract)

Feng, J. Y., Pei, X. Z., Yu, S. L., et al., 2010. The Discovery of the Mafic-Ultramafic Mélange in Kekesha Area of Dulan County, East Kunlun Region, and Its LA-ICP-MS Zircon U-Pb Age. *Geology in China*, 37: 28–38 (in Chinese with English Abstract)

Feng, C. Y., Wang, S., Li, G. C., et al., 2012. Middle to Late Triassic Granitoids in the Qimantagh Area, Qinghai Province, China: Chronology, Geochemistry and Metallogenic Significances. *Acta Petrologica Sinica*, 28: 665–678 (in Chinese with English Abstract)

Furman, T. Y., Bryce, J. G., Karson, J., et al., 2004. East African Rift System (EARS) Plume Structure: Insights from Quaternary Mafic Lavas of Turkana, Kenya. *Journal of Petrology*, 45(5): 1069–1088. https://doi.org/10.1093/petrology/egh004

Gao, X. F., Xiao, P. X., Xie, C. R., et al., 2010. Zircon LA-ICP-MS U-Pb Dating and Geological Significance of Bashierxi Granite in the Eastern Kunlun Area, China. *Geological Bulletin of China*, 29: 1001–1008 (in Chinese with English Abstract)

Guo, C. L., Chen, Y. C., Zeng, Z. L., et al., 2012. Petrogenesis of the Xihuashan Granites in Southeastern China: Constraints from Geochemistry and *in-situ* Analyses of Zircon U-Pb-Hf-O Isotopes. *Lithos*, 148: 209–227. https://doi.org/10.1016/j.lithos.2012.06.014

Hanyu, T., Tatsumi, Y., Nakai, S., et al., 2006. Contribution of Slab Melting and Slab Dehydration to Magmatism in the NE Japan Arc for the Last 25 Myr: Constraints from Geochemistry. *Geochemistry*, *Geophysics*, *Geosystems*, 7(8): 1–29. https://doi.org/10.1029/2005gc001220

Hao, J., Liu, X. H., Sang, H. Q., 2003. Geochemical Characteristics and $^{40}Ar/^{39}Ar$ Age of the Ayak Adamellite and Its Tectonic Significance in the East Kunlun, Xinjiang. *Acta Petrologica Sinica*, 19: 517–522 (in Chinese with English Abstract)

Hao, N. N., Yuan, W. M., Zhang, A. K., et al., 2015. Evolution Process of the Late Silurian–Late Devonian Tectonic Environment in Qimantagh in the Western Portion of East Kunlun, China: Evidence from the Geochronology and Geochemistry of Granitoids. *Journal of Earth System Science*, 124(1): 171–196. https://doi.org/10.1007/s12040-014-0531-z

Hofmann, A. W., 1988. Chemical Differentiation of the Earth: The Relationship between Mantle, Continental Crust, and Oceanic Crust. *Earth and Planetary Science Letters*, 90(3): 297–314. https://doi.org/10.1016/0012-821x(88)90132-x

Hoskin, P. W. O., Schaltegger, U., 2003. The Composition of Zircon and Igneous and Metamorphic Petrogenesis. *Reviews in Mineralogy and Geochemistry*, 53(1): 27–62. https://doi.org/10.2113/0530027

Irvine, T. N., Baragar, W. R. A., 1971. A Guide to the Chemical Classification of the Common Volcanic Rocks. *Canadian Journal of Earth Sciences*, 8(5): 523–548. https://doi.org/10.1139/e71-055

Jiang, C. F., Yang, J. S., Feng, B. G., 1992. Opening-Closing Evolution of the Kunlun Mountains. In: Jiang, C. F., Yang, J. S., Feng, B. G., eds., Opening Closing Tectonics of Kunlun Mountain. Geological Publishing House, Beijing (in Chinese)

Jiang, Y. H., Jia, R. Y., Liu, Z., et al., 2013. Origin of Middle Triassic High-K Calc-Alkaline Granitoids and Their Potassic Microgranular Enclaves from the Western Kunlun Orogen, Northwest China: A Record of the Closure of Paleo-Tethys. *Lithos*, 156–159: 13–30. https://doi.org/10.1016/j.lithos.2012.10.004

Ju, Y. J., Zhang, X. L., Lai, S. C., et al., 2017. Permian-Triassic Highly-Fractionated I-Type Granites from the Southwestern Qaidam Basin (NW China): Implications for the Evolution of the Paleo-Tethys in the Eastern Kunlun Orogenic Belt. *Journal of Earth Science*, 28(1): 51–62. https://doi.org/10.1007/s12583-017-0745-5

Kong, H. L., Li, J. C., Li, Y. Z., et al., 2017. Zircon LA-ICP-MS U-Pb Dating and Its Geological Significance of the Halongxiuma Pyroxene Peridotite in East Kunlun, Qinghai Province. *Geological Science and Technology Information*, 36: 41–47 (in Chinese with English Abstract)

Li, S. J., Sun, F. Y., Gao, Y. W., et al., 2012. The Theoretical Guidance and the Practice of Small Intrusions Forming Large Deposits: The Enlightenment and Significance for Searching Breakthrough of Cu-Ni Sulfide Deposit in Xiarihamu, East Kunlun, Qinghai. *Northwestern Geology*, 45(4): 185–191 (in Chinese with English Abstract)

Li, H. K., Lu, S. N., Xiang, Z. Q., et al., 2006. SHRIMP U-Pb Zircon Age of the Granulite from the Qingshuiquan Area, Central Eastern Kunlun Suture Zone. *Earth Science Frontiers*, 13: 311–321 (in Chinese with English Abstract)

Li, R. S., Ji, W. H., Yang, Y. C., et al., 2008. Kunlun Mountains and Geology of Adjacent Areas. Geological Publishing House, Beijing (in Chinese with English Abstract)

Li, X. T., Yan, D. P., Qiu, L., 2018. Early Cretaceous Post-Collisional Collapse of the Yidun Terrane: Geochronological and Geochemical Constraints from Calc-Alkaline to Alkaline Basalts in Xiqiu Area, Southwest China. *Journal of Earth Science*, 29(1): 57–77. https://doi.org/10.1007/s12583-018-0825-1

Li, Z. X., Bogdanova, S. V., Collins, A. S., et al., 2008. Assembly, Configuration, and Break-Up History of Rodinia: A Synthesis. *Precambrian Research*, 160: 179–210

Liu, B., Ma, C. Q., Jiang, H. A., et al., 2013a. Early Paleozoic Tectonic Transition from Ocean Subduction to Collisional Orogeny in the Eastern Kunlun Region: Evidence from Huxiaoqin Mafic Rocks. *Acta Petrologica Sinica*, 29: 2093–2106 (in Chinese with English Abstract)

Liu, B., Ma, C. Q., Guo, P., et al., 2013b. Discovery of the Middle Devonian A-Type Granite from the Eastern Kunlun Orogen and Its Tectonic Implications. *Earth Science*, 38(5): 947–962 (in Chinese with English Abstract)

Liu, B., Ma, C. Q., Zhang, J. Y., et al., 2012. Petrogenesis of Early Devonian Intrusive Rocks in the East Part of Eastern Kunlun Orogen and Implication for Early Paleozoic Orogenic Processes. *Acta Petrologica Sinica*, 28: 1785–1807 (in Chinese with English Abstract)

Liu, Y. H., Mo, X. X., Yu, X. H., et al., 2006. Zircon SHRIMP U-Pb Dating of the Jingren Granite, Yemaquan Region of the East Kunlun and Its Geological Significance. *Acta Petrologica Sinica*, 22: 2457–2463 (in Chinese with English Abstract)

Liu, Y. S., Hu, Z. C., Gao, S., et al., 2008. *In-situ* Analysis of Major and Trace Elements of Anhydrous Minerals by LA-ICP-MS without Applying an Internal Standard. *Chemical Geology*, 257(1/2): 34–43. https://doi.org/10.1016/j.chemgeo.2008.08.004

Liu, Z. Q., Pei, X. Z., Li, R. B., et al., 2011. LA-ICP-MS Zircon U-Pb Geochronology of the Two Suites of Ophiolites at the Buqingshan Area of the A'nyemaqen Orogennic Belt in the Southern Margin of East Kunlun and Its Tectonic Implication. *Acta Geologica Sinica*, 85: 185–194 (in Chinese with English Abstract)

Lu, J. P., Dai, M. F., Li, J., et al., 2006. Geochemical Characteristics and Its Tectonic Setting of Xiremangya Late Carboniferous Granite in the Qimantagh Mountains, East Kunlun. *Geology and Mineral Resources of South China*, 4: 1–8 (in Chinese with English Abstract)

Lu, S. N., 2002. Precambrian Geology of the Northern Qinghai-Tibet Plateau. Geological Publishing House, Beijing (in Chinese)

Lu, S. N., 2001. From Rodinia to Gondwanaland Supercontinents-Thinking about Problems of Researching Neoproterozoic Supercontinents. *Earth Science Frontiers*, 8(4): 441–448 (in Chinese with English Abstract)

Ludwig, K. R., 2003. User's Manual for Isoplot/Ex v30: A Geochronology Toolkit for Microsoft Excel. *Berkeley Geochronological Center Special Publications*, 4: 25–31

Ma, Y. S., Bai, Y. S., He, J., et al., 2010. Discovery of Erchang Granite in Qimantagh Region in Pan-African Period and Its Significance. *Journal of Qinghai University*, 28: 56–60 (in Chinese with English Abstract)

MacDonald, R., 2001. Plume-Lithosphere Interactions in the Generation of the Basalts of the Kenya Rift, East Africa. *Journal of Petrology*, 42(5): 877–900. https://doi.org/10.1093/petrology/42.5.877

McDonough, W. F., Sun, S. S., 1995. The Composition of the Earth. *Chemical Geology*, 120(3/4): 223–253. https://doi.org/10.1016/0009-2541(94)00140-4

McKenzie, D., 1989. Some Remarks on the Movement of Small Melt Fractions in the Mantle. *Earth and Planetary Science Letters*, 95(1/2): 53–72. https://doi.org/10.1016/0012-821x(89)90167-2

Meng, F. C., Zhang, J. X., Cui, M. H., 2013. Discovery of Early Paleozoic Eclogite from the East Kunlun, Western China and Its Tectonic Significance. *Gondwana Research*, 23(2): 825–836. https://doi.org/10.1016/j.gr.2012.06.007

Mo, X. X., Luo, Z. H., Deng, J. F., et al., 2007. Granitoids and Crustal Growth in the East-Kunlun Orogenic Belt. *Geological Journal of China Universities*, 13: 403–414 (in Chinese with English Abstract)

Neal, C. R., 2002. Mantle Sources and the Highly Variable Role of Continental Lithosphere in Basalt Petrogenesis of the Kerguelen Plateau and Broken Ridge LIP: Results from ODP Leg 183. *Journal of Petrology*, 43(7): 1177–1205. https://doi.org/10.1093/petrology/43.7.1177

Pan, Y. S., Zhou, W. M., Xu, R. H., et al., 1996. Geological Characteristics and Evolution of the Kunlun Mountains Region during the Early Paleozoic. *Science in China*: *Earth Sciences*, 4: 302–307 (in Chinese)

Pearce, J. A., Peate, D. W., 1995. Tectonic Implications of the Composition of Volcanic Arc Magmas. *Annual Review of Earth and Planetary Sciences*, 23(1): 251–285. https://doi.org/10.1146/annurev.ea.23.050195.001343

Peccerillo, A., Taylor, S. R., 1976. Geochemistry of Eocene Calc-Alkaline Volcanic Rocks from the Kastamonu Area, Northern Turkey. *Contributions to Mineralogy and Petrology*, 58(1): 63–81. https://doi.org/10.1007/bf00384745

Peng, B., Sun, F. Y., Li, B. L., et al., 2016. The Geochemistry and Geochronology of the Xiarihamu II Mafic-Ultramafic Complex, Eastern Kunlun, Qinghai Province, China: Implications for the Genesis of Magmatic Ni-Cu Sulfide Deposits. *Ore Geology Reviews*, 73: 13–28. https://doi.org/10.13039/501100004613

Regelous, M., Collerson, K. D., Ewart, A., et al., 1997. Trace Element Transport Rates in Subduction Zones: Evidence from Th, Sr and Pb Isotope Data for Tonga-Kermadec Arc Lavas. *Earth and Planetary Science Letters*, 150(3/4): 291–302. https://doi.org/10.1016/s0012-821x(97)00107-6

Rudnick, R. L., Fountain, D. M., 1995. Nature and Composition of the Continental Crust: A Lower Crustal Perspective. *Reviews of Geophysics*, 33(3): 267–309. https://doi.org/10.1029/95rg01302

Sang, J. Z., Pei, X. Z., Li, R. B., et al., 2016. LA-ICP-MS Zircon U-Pb Dating and Geochemical Characteristics of Gabbro in Qingshuiquan, East Section of East Kunlun, and Its Tectonic Significance. *Geological Bulletin of China*, 35: 700–710 (in Chinese with English Abstract)

Shen, Y. C., Yang, J. Z., Wang, Y. J., et al., 1999. Petrologic Characteristics and Tectonic Setting of Volcanic Rocks Upper Triassic System in the Qimantagh Region in East Kunlun Orogenic Belt, Xinjiang. *Geotectonica et Metallogenia*, 79: 50–58 (in Chinese with English Abstract)

Song, X. Y., Yi, J. N., Chen, L. M., et al., 2016. The Giant Xiarihamu Ni-Co Sulfide Deposit in the East Kunlun Orogenic Belt, Northern Tibet Plateau, China. *Economic Geology*, 111(1): 29–55. https://doi.org/10.2113/econgeo.111.1.29

Song, X. Y., Yi, J. N., Chen, L. M., et al., 2016. The giant Xiarihamu Ni-Co Sulfide Deposit in the East Kunlun Orogenic Belt, Northern Tibet Plateau, China. *Economic Geology*, 111(1): 29–55. https://doi.org/10.2113/econgeo.111.1.29

Sun, F. Y., Li, B. L., Ding, Q. F., et al., 2009. Research on the Key Problems of Ore Prospecting in the Eastern Kunlun Metallogenic Belt. Geological Survey Institute of Jilin University, Changchun (in Chinese)

Sun, S. S., McDonough, W. F., 1989. Chemical and Isotopic Systematics of Oceanic Basalts: Implications for Mantle Composition and Processes. *Geological Society*, *London*, *Special Publications*, 42(1): 313–345. https://doi.org/10.1144/gsl.sp.1989.042.01.19

Tan, S. X., Bai, Y. S., Chang, G. H., et al., 2004. Discovery and Geological Significance of Metamorphic and Intrusive Rock (System) of Qimantagh Region in Jinning Epoch. *Northwestern Geology*, 37: 69–73 (in Chinese with English Abstract)

Wang, B. Z., Luo, Z. H., Li, H. Y., et al., 2009. Petrotectonic Assemblages and Temporal-Spatial Framework of the Late Paleozoic–Early Mesozoic Intrusions in the Qimantagh Corridor of the East Kunlun Belt. *Geology in China*, 36: 769–782 (in Chinese with English Abstract)

Wang, B. Z., Luo, Z. H., Pan, T., et al., 2012. Petrotectonic Assemblages and LA-ICP-MS Zircon U-Pb Age of Early Paleozoic Volcanic Rocks in Qimantagh Area, Tibetan Plateau. *Geological Bulletin of China*, 31: 860–874 (in Chinese with English Abstract)

Wang, G., Sun, F. Y., Li, B. L., et al., 2014. Petrography, Zircon U-Pb Geochronology and Geochemistry of the Mafic-Ultramafic Intrusion in Xiarihamu Cu-Ni Deposit from East Kunlun, with Implications for Geodynamic Setting. *Earth Science Frontiers*, 21(6): 381–401 (in Chinese with English Abstract)

Wang, G., Sun, F. Y., Li, B. L., et al., 2013. Zircon U-Pb Geochronology and Geochemistry of the Early Devonian Syenogranite in the Xiarihamu Ore District from East Kunlun, with Implications for the Geodynamic Setting. *Geotectonica et Metallogenia*, 37(4): 685–697401 (in Chinese with English Abstract)

Wang, G. C., Wei, Q. R., Jia, C. X., et al., 2007. Some Ideas of Precambrian Geology in the East Kunlun, China. *Geological Bulletin of China*, 26(8): 929–937 (in Chinese with English Abstract)

Watson, E. B., 1979. Zircon Saturation in Felsic Liquids: Experimental Results and Applications to Trace Element Geochemistry. *Contributions to Mineralogy and Petrology*, 70(4): 407–419. https://doi.org/10.1007/bf00371047

Watson, E. B., Harrison, T. M., 1983. Zircon Saturation Revisited: Temperature and Composition Effects in a Variety of Crustal Magma Types. *Earth and Planetary Science Letters*, 64(2): 295–304. https://doi.org/10.1016/0012-821x(83)90211-x

Whalen, J. B., Currie, K. L., Chappell, B. W., 1987. A-Type Granites: Geochemical Characteristics, Discrimination and Petrogenesis. *Contributions to Mineralogy and Petrology*, 95(4): 407–419. https://doi.org/10.1007/bf00402202

Wu, F. Y., Jahn, B. M., Wilde, S., et al., 2000. Phanerozoic Crustal Growth: U-Pb and Sr-Nd Isotopic Evidence from the Granites in Northeastern China. *Tectonophysics*, 328(1/2): 89–113. https://doi.org/10.1016/s0040-1951(00)00179-7

Wu, F. Y., Wilde, S. A., Zhang, G. L., et al., 2004. Geochronology and Petrogenesis of the Post-Orogenic Cu-Ni Sulfide-Bearing Mafic-Ultramafic Complexes in Jilin Province, NE China. *Journal of Asian Earth Sciences*, 23(5): 781–797. https://doi.org/10.1016/s1367-9120(03)00114-7

Wu, F. Y., Yang, Y. H., Xie, L. W., et al., 2006. Hf Isotopic Compositions of the Standard Zircons and Baddeleyites Used in U-Pb Geochronology. *Chemical Geology*, 234(1/2): 105–126. https://doi.org/10.1016/j.chemgeo.2006.05.003

Wu, F. Y., Li, X. H., Yang, J. H., et al., 2007. Discussions on the Petrogenesis of Granites. *Acta Petrolei Sinica*, 23(6): 1217–1238 (in Chinese with English Abstract)

Yan, W., Qiu, D. M., Ding, Q. F., et al., 2016. Geochronology, Petrogenesis, Source and Its Structural Significance of Houtougou Monzogranite of Wulonggou Area in Eastern Kunlun Orogen. *Journal of Jilin University*, 46(2): 443–460 (in Chinese with English Abstract)

Yang, J. S., Robinson, P. T., Jiang, C. F., et al., 1996. Ophiolites of the Kunlun Mountains, China and Their Tectonic Implications. *Tectonophysics*, 258(1–4): 215–231. https://doi.org/10.1016/0040-1951(95)00199-9

Yuan, H. L., Gao, S., Liu, X. M., et al., 2004. Accurate U-Pb Age and Trace Element Determinations of Zircon by Laser Ablation-Inductively Coupled Plasma-Mass Spectrometry. *Geostandards and Geoanalytical Research*, 28(3): 353–370. https://doi.org/10.1111/j.1751-908x.2004.tb00755.x

Zhang, Y. L., Hu, D. G., Shi, Y. R., et al., 2010. SHIRMP Zircon U-Pb Ages and Tectonic Significance of Maoniushan Formation Volcanic Rocks in East Kunlun Orogenic Belt, China. *Geological Bulletin of China*, 29: 1614–1618 (in Chinese with English Abstract)

Zhao, X., Fu, L. B., Wei, J. H., et al., 2018. Geochemical Characteristics of An'nage Hornblende Gabbro from East Kunlun Orogenic Belt and Its Constraints on Evolution of Paleo-Tethys Ocean. *Earth Science*, 43(2): 354–370 (in Chinese with English Abstract). https://doi.org/10.3799/dqkx.2018.020

Zhao, Z. M., Ma, H. D., Wang, B. Z., et al., 2008. The Evidence of Intrusive Rocks about Collision-Orogeny during Early Devonian in Eastern Kunlun Area. *Geological Review*, 54: 47–56 (in Chinese with English Abstract)

Zhu, C. B., Sun, F. F., Yuan, W. M., et al., 2018. Apatite Fission Track Thermochronology and Tectonic Significance in Yemaquan Area, East Kunlun. *Earth Science*, 43(6): 2019–2028 (in Chinese with English Abstract). https://doi.org/ 10.3799/dqkx.2018.598

Zhu, Y. H., Lin, Q. X., Jia, C. X., et al., 2006. SHRIMP Zircon U-Pb Age and Significance of Early Paleozoic Volcanic Rocks in East Kunlun Orogenic Belt, Qinghai Province, China. *Science China Earth Sciences*, 49(1): 88–96. https://doi.org/10.1007/s11430-004-5317-8

Zhu, Y. H., Lin, Q. X., Jia, C. X., et al., 2005. Early Paleozoic Volcanic Zircon SHRIMP Age and Its Geological Significance of East Kunlun Orogenic Belt. *Science in China Series D*: *Earth Sciences*, 35: 1112–1119 (in Chinese with English Abstract)